Journal of
Applied Remote Sensing

Assessment of particulate absorption properties in the southeastern Bering Sea from in-situ and remote sensing data

Puneeta Naik
Eurico J. D'Sa
Joaquim I. Goés
Helga R. Gomes

Assessment of particulate absorption properties in the southeastern Bering Sea from in-situ and remote sensing data

Puneeta Naik,[a] Eurico J. D'Sa,[a] Joaquim I. Goés,[b] and Helga R. Gomes[b]

[a] Louisiana State University, Department of Oceanography and Coastal Sciences, Coastal Studies Institute, 306 Howe-Russell Geoscience Complex, Baton Rouge, LA 70803
pnaik2@tigers.lsu.edu, ejdsa@lsu.edu

[b] Bigelow Laboratory for Ocean Sciences, 180 McKown Point Road, West Boothbay Harbor, ME 04575
jgoes@bigelow.org, hgomes@bigelow.org

Abstract. Particulate absorption ($a_P(\lambda)$) including phytoplankton ($a_{PHY}(\lambda)$) and non-algal particles (NAP) ($a_{NAP}(\lambda)$) were measured in southeastern Bering Sea during a cruise in July 2008. This study analyzes the $a_P(\lambda)$ properties through in-situ and quasi analytical algorithm (QAA) derived ocean color satellite Medium Resolution Imaging spectrometer (MERIS) and Moderate resolution Imaging Spectroradiometer (MODIS) observations. We found that the $a_P(\lambda)$ and $a_{PHY}(\lambda)$ correlated well with chlorophyll-a and were lower as a function of chlorophyll-a as compared to low latitudes. The specific phytoplankton absorption ($a^*_{PHY}(\lambda)$) showed more variability in the blue as compared to the red part of the spectrum indicating pigment packaging and/or change in pigment composition. The remote sensing reflectance ($R_{rs}(\lambda)$) showed significant variability in spectral shape and magnitude which was consistent with the variable total absorption minus pure water absorption ($a_{T-W}(\lambda)$) spectra observed in the study area. Simple satellite retrieved $R_{rs}(\lambda)$ ratios were related to in-situ $a_{PHY}(\lambda)$ and $a_{DG}(\lambda)$ by applying an inverse power fit; $R_{rs}(490)/R_{rs}(510)$ gave the best results for $a_{PHY}(443)$ and $a_{DG}(443)$ (R^2 - 0.80 and 0.75) respectively. The match-ups of in-situ and MERIS retrieved $a_{PHY}(\lambda)$ and NAP plus colored dissolved organic matter ($a_{DG}(\lambda)$) using QAA after log-transformation showed reasonable agreement with R^2 of 0.71 and 0.61 and RMSE of 0.316 and 0.391 at 443 nm, respectively. Although the QAA derived $a_{PHY}(\lambda)$ and $a_{DG}(\lambda)$ from MERIS overestimated and underestimated, respectively the in-situ measurements at all wavelengths, the match-up analysis was encouraging.

Keywords: Light absorption, particulate, phytoplankton, non-algal particles, quasi analytical algorithm (QAA), Bering Sea.

1 INTRODUCTION

In recent decades satellites have offered synoptic views across large spatial and temporal scales in the global oceans. Ocean color sensors such as MODIS and SeaWiFS have shown the utility of using ocean color data for understanding the oceans role in global biogeochemical cycles. Although ocean color imagery have shown that high-latitude oceans are among the most productive in the world, but very few in-situ observations are present to validate and quantify the satellite observations. Also frequent cloud and ice cover reduce good imagery and contaminate retrieval of biogeochemical variables from ocean reflectance observations. The above constraints along with difficulties in atmospheric corrections at high latitudes have limited the usefulness of ocean color imagery. Recently the ocean color community has directed its attention towards such high latitude regions as the sensitivity of these regions under climate changing scenarios needs to be understood [1,2].

Received 4 Mar 2010; accepted 12 Nov 2010; published 19 Nov 2010 [CCC: 19313195/2010/$25.00]

Absorption coefficients are very important bio-optical properties in the study of primary production, carbon flux [3], water quality [4] and even physical processes in the ocean [5]. The total absorption coefficient of seawater is the sum of individual components within the water column, namely colored dissolved organic matter (CDOM), phytoplankton and non-algal particulate matter (NAP) and can be expressed as

$$a_T(\lambda) = a_W(\lambda) + a_{CDOM}(\lambda) + a_{PHY}(\lambda) + a_{NAP}(\lambda)$$

$$a_P(\lambda) = a_{PHY}(\lambda) + a_{NAP}(\lambda)$$

where $a_W(\lambda)$, $a_{CDOM}(\lambda)$, $a_{PHY}(\lambda)$, $a_{NAP}(\lambda)$ and $a_P(\lambda)$ are absorption coefficients due to pure water, CDOM, phytoplankton, non-algal particulate matter and particulate matter, respectively.

Chlorophyll distributions and primary productivity studies illustrate that the Bering Sea is a highly productive region, with primary productivity ranging from 175–275 g C m^{-2} yr^{-1} near the shelf break also known as the 'greenbelt' [6]. The absorption of light by particulate and dissolved matter transforms the sub-surface light field and is important for estimation of primary productivity from remote sensing over large spatial and temporal scales. Such data on a decadal scale provides a synoptic view which can be used to study variability due to climate shifts. The Bering Sea has been subjected to such large scale climatic variations that have led to large variations in biology of the region [7]. Bio-optical data in the Bering Sea have very limited spatial and temporal coverage. Recently conducted studies have shown seasonal and inter-annual variability of chlorophyll-a from monthly SeaWiFS climatologies (http://seawifs.gsfc.nasa.gov) for 1998–2002 [8].

The southeastern Bering Sea shelf waters during summer can be characterized by their hydrographic structure and currents into three domains, coastal (<50 m depth), middle (50 - 100 m depth) and outer (100 - 200 m depth) domain [9] (Fig. 1). The shelf is broad and shallow with a steep shelf break and during summer changes in water column density are driven by temperature rather than by salinity. The coastal domain under the influence of tidal and wind mixing is well mixed, the middle domain is characterized by a tidally mixed lower layer and a well mixed surface layer as warm surface waters together with low wind energy cause inefficient wind mixing of the water column. The outer shelf domain is similar to the middle domain except that the wind-mixed surface layer and a tidally mixed bottom layer are separated by a transition layer.

Previous studies on bio-optical properties in high latitudes focused on the impact of the absorption properties on the retrieval of chlorophyll-a primarily from in-situ remote sensing reflectance ($R_{rs}(\lambda)$) data, with little or no utilization of $R_{rs}(\lambda)$ from satellite data [1, 2]. Further, these studies did not attempt to match-up in-situ and satellite retrieved absorption products. The main goal of this study is to test the potential of Lee et al., (2002) [10] Quasi Analytical Algorithm (QAA) for retrieval of absorption (phytoplankton and non-algal particulate plus CDOM absorption) using MERIS and MODIS ocean color satellites. The main objectives of this study are (1) describe the variability of particulate absorption in the study region which control the variability in $R_{rs}(\lambda)$, (2) describe particulate ($a_P(\lambda)$), phytoplankton ($a_{PHY}(\lambda)$) and specific phytoplankton ($a^*_{PHY}(\lambda)$) absorption in relation to chlorophyll-a, (3) conduct match-up of in-situ and QAA retrieved absorption coefficients, and (4) relate simple two band $R_{rs}(\lambda)$ ratio to the in-situ absorption coefficients in the study area.

2 METHODS

2.1 In-situ water sampling

Station locations that were sampled are shown in Fig. 1. Sampling was conducted along cross shelf as well as along shelf transects covering the coastal, middle and outer domain during a

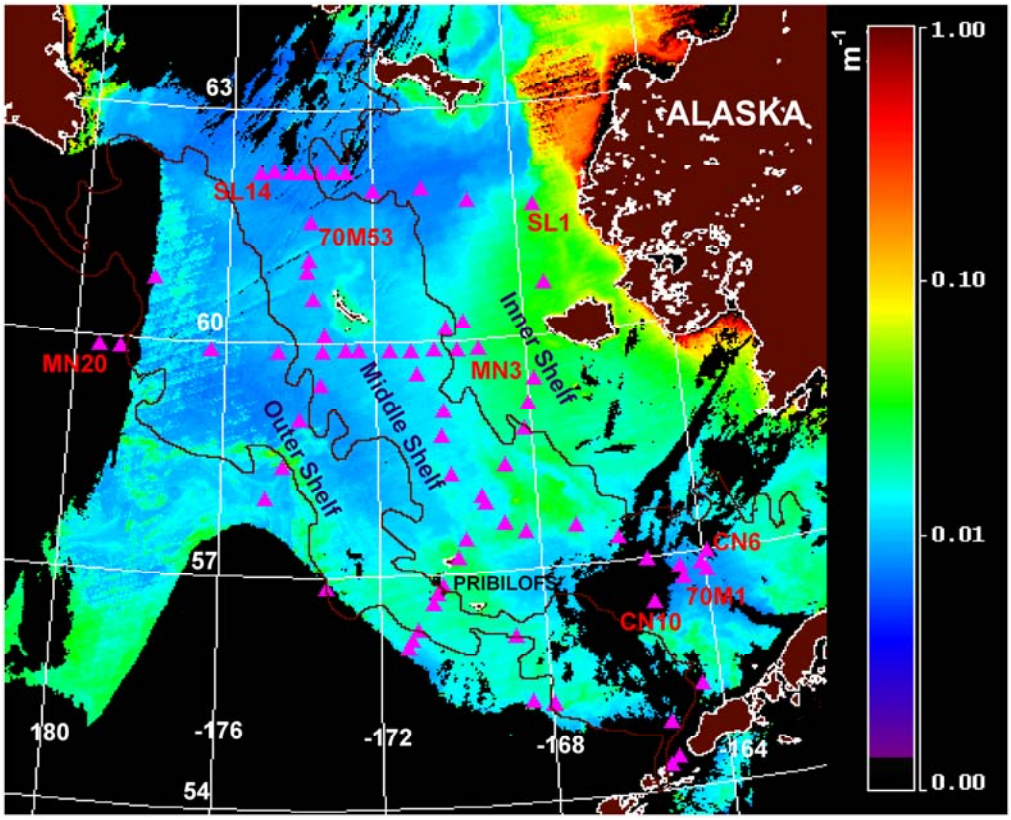

Fig. 1. Locations of stations sampled during the cruise in July 2008 overlaid on a MODIS Aqua QAA - $a_{PHY}(443)$ image collected on July, 7, 2008.

cruise in July 2008. At every station, salinity, temperature and density profiles were recorded with a SeaBird SBE-911 plus CTD unit and water samples were collected for absorption analyses at the surface using Niskin bottles attached to the CTD.

2.2 Absorption – Phytoplankton, NAP and CDOM

Particulate absorption was determined using the standard QFT procedure [11]. The discrete water samples were filtered under low vacuum on 0.7μm Whatman GF/F glass fiber filters and stored in liquid nitrogen until analysis for particulate absorption and chlorophyll-a. The volume to be filtered ranged from 100 – 2000 ml and care was taken not to overload the filter.

For particulate absorption, samples were first thawed to room temperature after removing from liquid nitrogen by keeping them in the dark at room temperature for half an hour. Filter paper blanks were prepared by filtering 15 ml of filtered seawater corresponding to the station under analysis. Absorbance measurements of total particulate matter ($A_P(\lambda)$) were done by scanning the sample filter paper using a shipboard WPI Ultrapath™ hyperspectral waveguide capillary system from 190 – 722 nm at 1 nm intervals. The absorbance was converted to absorption coefficient by using the equation given below

$$a_P(\lambda) = \frac{2.303\left[A_P(\lambda)\right]}{(V/A)}$$

where $a_P(\lambda)$ (m^{-1}) is the total particulate absorption, V (m^3) is the volume filtered, and A (m^2) the area of the filter paper.

To separate the phytoplankton pigments within the particulate matter from NAP, methanol extraction was done [12]. The sample filter paper was scanned again following the procedure described above to obtain non-algal particulate (NAP) absorbance ($A_{NAP}(\lambda)$). $A_{NAP}(\lambda)$ was converted to $a_{NAP}(\lambda)$ using the equation shown above. The phytoplankton absorption ($a_{PHY}(\lambda)$ (m^{-1})) spectra were obtained by subtracting the $a_{NAP}(\lambda)$ (m^{-1}) from $a_P(\lambda)$ using the relation

$$a_{PHY}(\lambda) = a_P(\lambda) - a_{NAP}(\lambda)$$

To correct for residual and scattering offsets in the absorption measurements the mean value from 700 – 722 nm was subtracted from the entire spectra [13] and the Cleveland and Weidemann (1993) [14] procedure was utilized to correct for pathlength amplification. Chlorophyll-a specific phytoplankton absorption ($a^*_{PHY}(\lambda)$ (m^2 (mg chl a)$^{-1}$)) was obtained by dividing $a_{PHY}(\lambda)$ by chlorophyll-a (mg m^{-3}). Chlorophyll-a concentrations were determined fluorometrically with 90% acetone [15] in a Turner Designs fluorometer.

For CDOM absorption ($a_{CDOM}(\lambda)$), discrete water samples were filtered immediately after collection through 0.2 μm nucleopore membrane filters under low vacuum. Filtered samples were stored in acid cleaned, pre-combusted amber colored glass bottles and stored at 4 ^oC. The filtered samples were allowed to reach ambient room temperature to minimize temperature bias between samples and blank (Milli-Q water). Absorbance measurements of CDOM ($A_{CDOM}(\lambda)$) were done on a shipboard hyperspectral waveguide capillary system from 190 – 722 nm at 1 nm intervals using Milli-Q water as blank. The absorbance data were corrected for baseline fluctuations by subtraction of the mean value over 5 nm interval of the measured absorbance at 700 nm from each wavelength [13]. The $a_{CDOM}(\lambda)$ (m^{-1}) for pathlength, L (m^{-1}) was calculated according to

$$a_{CDOM}(\lambda) = \frac{2.303[A_{CDOM}(\lambda)]}{(L)}$$

2.3 Remote sensing data – MERIS and MODIS aqua imagery

Level 1 MODIS Aqua imagery from July 3 - July 31, 2008 was obtained from the OBPG NASA Ocean Color website (http://oceancolor.gsfc.nasa.gov/) and was processed to Level 2 using the SeaDAS 5.3 software package. The standard atmospheric correction algorithm was used which is based on the Gordon and Voss (1999) approach [16]. The pixels were masked out after atmospheric correction by the following flags: land, cloud or ice, high top-of-atmosphere radiance, low normalized water-leaving radiance at 551 nm, stray light, sun-glint, or atmospheric correction failure. The MERIS Level 2 data was obtained from the ESA website (http://merci-srv.eo.esa.int/merci/) and processed using BEAM 4.5.3 software. The documentation for MERIS products and atmospheric correction algorithms used for processing of data from Level 1 to Level 2 can be found at the ESA website (http://earth.esa.int/pcs/envisat/meris/documentation/). The Lee et al. (2002) QAA (version 5) [10, http://www.ioccg.org/groups/Software_OCA/QAA_v5.pdf] was used to derive absorption products from satellite $R_{rs}(\lambda)$ (sr^{-1}). The QAA was selected amongst other semi-analytical models (e.g. GSM, Carder) as it generated greater positive values of absorption and least number of algorithm failure pixels. The QAA retrieves $a_{PHY}(\lambda)$ but does not retrieve $a_{NAP}(\lambda)$, however it retrieves a combination of NAP and CDOM absorption ($a_{DG}(\lambda)$). Hence for analyses of in-situ and remote sensing of $a_{DG}(\lambda)$, the in-situ $a_{CDOM}(\lambda)$ was added to in-situ $a_{NAP}(\lambda)$ to obtain in-situ $a_{DG}(\lambda)$. A 3 x 3 pixel box size (1.2 km/pixel for MERIS and 1 km/pixel for MODIS) with a time difference of ±8 hours between the in-situ sampling and satellite overpass was chosen for in-situ and satellite data match-up analyses.

3 RESULTS AND DISCUSSION

3.1 Spatial distribution of in-situ $a_{PHY}(443)$, $a_{NAP}(443)$ and $a_P(443)$

The $a_{PHY}(443)$, $a_{NAP}(443)$, and $a_P(443)$ reveal a range from 0.004 – 0.097 m^{-1}, 0.002 – 0.048 m^{-1}, and 0.007 – 0.112 m^{-1} in the study area, respectively. The surface distribution of $a_{PHY}(443)$ revealed relatively higher $a_{PHY}(443)$ around the Pribilof Islands which is mostly due to the enhanced production near the islands caused by interaction of tides and currents with bathymetry [9,17] (Fig. 2). The highest values were observed near the Pribilof Islands and the lowest values on the northern part of the outer-shelf (Fig. 2a). The $a_{NAP}(443)$ surface distribution generally showed higher values closer to the coast and lower values were seen on the outer-shelf except near the Pribilofs where there seems to be some influence of elevated biomass on $a_{NAP}(443)$ (Fig. 2b). The relative contribution of $a_{PHY}(443)$ and $a_{NAP}(443)$ to $a_P(443)$ was highly variable and ranged from 15% - 90% and 10% - 85% respectively, suggesting that different parts of the study region have variable contributions from $a_{PHY}(443)$ and $a_{NAP}(443)$. Fig. 2c shows this variability in terms of $a_{PHY}(443)$ by $a_P(443)$ ratio; the inner-shelf shows the least and the middle-shelf the highest contribution of $a_{PHY}(443)$ to $a_P(443)$. The northern part of the outer-shelf shows lower contribution of $a_{PHY}(443)$ to $a_P(443)$ as compared to the southern part. On average the contribution from $a_{PHY}(443)$ was higher

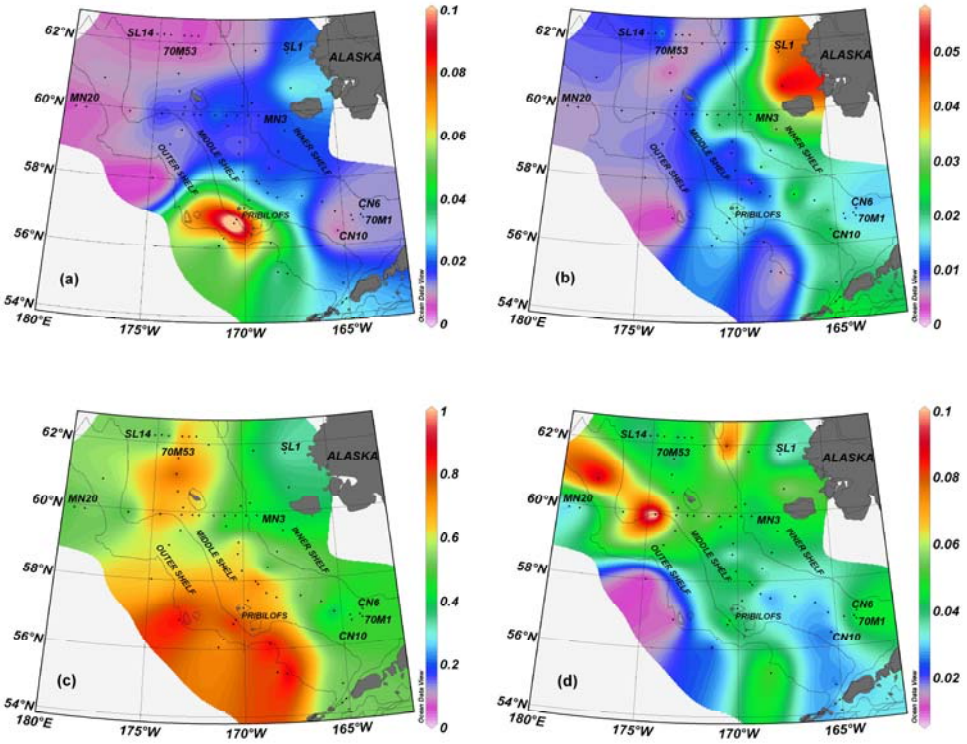

Fig. 2. Surface distribution of (a) phytoplankton absorption, $a_{PHY}(443)$ (m^{-1}) (b) Non-algal/detrital absorption, $a_{NAP}(443)$ (m^{-1}), (c) ratio of phytoplankton and total particulate absorption, $a_{PHY}(443)/a_P(443)$ and (d) chlorophyll-a specific phytoplankton absorption, $a^*_{PHY}(443)$ (m^2 (mg chl *a*)$^{-1}$) at 443 nm.

(~ 65%) as compared to $a_{NAP}(443)$ (~ 35%) to $a_P(443)$. A relatively higher correlation between $a_{PHY}(443)$ and $a_P(443)$ ($R^2 = 0.80$, n = 45, $p<0.001$), and lower correlation between $a_{NAP}(443)$ and $a_P(443)$ ($R^2 = 0.65$, n = 45, $p<0.001$) was observed in the study area.

The $a^*_{PHY}(443)$ surface distribution shows large variability and is far from being constant (Fig. 2d). In general the southern part of the study region showed lower values as compared to the northern part of the study region. High values (> 0.06 m^2 (mg chl *a*)$^{-1}$) are observed where the chlorophyll-a concentration is < 0.2 mg m^{-3} and low values (< 0.06 m^2 (mg chl *a*)$^{-1}$) are observed where the chlorophyll-a concentration is > 0.2 mg m^{-3}. The high values indicate a low packaging effect and/or change in pigment composition. A detailed description on the spatial distribution of absorption coefficients across and along the shelf is covered in Naik et al. (2009a) [18] and Naik et al. (2009b) [19], respectively.

3.2 In-situ $a_{PHY}(443)$, $a_P(443)$ relation with chlorophyll-a

A power function is applied to $a_{PHY}(443)$, $a_P(443)$ and chlorophyll-a relationship in accordance with Bricaud et al., (1998) [20] to investigate $a_{PHY}(443)$ and $a_P(443)$ in the southeastern Bering Sea in comparison to other regions (Fig. 3). We found a good correlation between $a_{PHY}(443)$, $a_P(443)$, and chlorophyll-a consistent with studies done both in the higher latitudes [1,21] as well as lower latitudes [20] (Table 1).

The Bricaud et al., 1998 [20] exponents for $a_{PHY}(443)$ and $a_P(443)$ are lower whereas the amplitude is higher for $a_{PHY}(443)$ and lower for $a_P(443)$ compared to our study. The power fit applied to $a_{PHY}(443)$ and chlorophyll-a for our data is significantly different (t-test, $p < 0.001$) from the Bricaud et al., 1998 [20] fit. The coefficients of the fit for $a_{PHY}(443)$ and chlorophyll-a obtained for our study are remarkably close to those found by Matsuoka et al. (2007) [21] in western Arctic Ocean. This suggests that methodological differences involved in obtaining $a_{PHY}(443)$ through the QFT method are not an issue and the trends seen are characteristic of these high latitude oceans. One reason attributed for the difference between higher and lower latitudes is due to change in pigment composition and/or pigment packaging; the separation of these effects is difficult in natural water samples [20,21]. These effects are explored through the $a^*_{PHY}(\lambda)$ and chlorophyll-a in the next section. This emphasizes a need for a regional/seasonal approach to ocean color algorithm development and applications. Although high correlation and tendency of increasing $a_{PHY}(\lambda)$ with chlorophyll-a is comparable with Bricaud et al., 1998 [20], a systematic departure is seen over the entire range of chlorophyll-a between our fit and Bricaud et al., 1998 [20] fit.

In order to investigate these difference further, we observed the variability in $a_{PHY}(\lambda)$ at the blue and red part of the spectrum. The $a_{PHY}(\lambda)$ was highly variable in the blue part of the spectrum (e.g., 0.004 - 0.097 m^{-1} at 443 nm) as compared to the red part of the spectrum (e.g., 0.001 - 0.016 m^{-1} at 667 nm); an additional indication of change in pigment composition or pigment package effect [20,22]. The trends for $a_P(443)$ versus chlorophyll-a for the above mentioned studies are not significantly different from each other. The non-linearity in the trend is mainly at lower chlorophyll-a values where the contribution from $a_{PHY}(443)$ and $a_{NAP}(443)$ is almost equal at some stations (Fig. 2c). The contribution of $a_{PHY}(443)$ and $a_{NAP}(443)$ to $a_P(443)$ is highly variable at lower chlorophyll-a concentrations (< 0.5 mg m^{-3}). From the difference in coefficients of the power fit applied for $a_{PHY}(443)$ and $a_P(443)$ we saw that the $a_{NAP}(443)$ made a considerable contribution to the observed relation. Further, the ratio of $a_{NAP}(\lambda)$ to $a_P(\lambda)$ at 443 nm showed an inverse relation with chlorophyll-a (Fig. 3c) arguing that an increase in $a_{NAP}(443)$ relative to $a_{PHY}(443)$ in low chlorophyll-a regions is responsible for the observed trend between $a_P(443)$ and chlorophyll-a. In general, the $a_{PHY}(443)$ and $a_P(443)$ as a function of chlorophyll-a are lower in the study region as compared to other mainly lower latitude regions, consistent with studies done at higher latitudes [20-22].

3.3 In-situ $a^*_{PHY}(443)$ relation with chlorophyll-a

Variations in light level, nutrients and phytoplankton species composition cause seasonal and regional variation of $a^*_{PHY}(\lambda)$ [23]. For our study region we found a large variation in $a^*_{PHY}(\lambda)$ spectra with variability greater in the blue (0.005 – 0.120 m^2 (mg chl *a*)$^{-1}$ at 443 nm) than the red region of the spectrum (0.003 – 0.0302 m^2 (mg chl *a*)$^{-1}$ at 676 nm) (Fig. 4a) [18,19].

The $a^*_{PHY}(676)$ variability can be mainly attributed to package effect, but variations in $a^*_{PHY}(443)$ may be due to package effect and/or changes in pigment composition [24]. As we observed more variability at 443 nm than at 676 nm, change in pigment composition may be the key source of variability of $a^*_{PHY}(\lambda)$. A decreasing trend of $a^*_{PHY}(443)$ from 0.120 - 0.005 m^2 (mg chl *a*)$^{-1}$ is observed with increasing chlorophyll-a concentration from 0.05 – 2 mg m^{-3} (Fig. 4b). The Bricaud et al., (1995) [25] fit is higher than the fit obtained for our study for almost the whole range of chlorophyll-a concentration. This indicates that $a^*_{PHY}(443)$ is consistently lower for our study as compared to Bricaud et al., (1995) [25] study, further indicating that change in pigment composition and/or change in pigment packaging exist in our study region consistent with studies done at higher latitudes [21,22]. In particular the blue to red ratio of $a^*_{PHY}(\lambda)$ for e.g., $a_{PHY}^*(443)/a_{PHY}^*(676)$ in this study varied from 6.9 to 1.1 demonstrating approximately a 6 fold decrease as chlorophyll-a increased from 0.08 to 1.46 mg m^{-3}. The $a_{PHY}^*(443)/a_{PHY}^*(676)$ inverse relation with chlorophyll-a is consistent with Bricaud et al. (1995) [25]. This ratio is found to be strongly correlated with the ratio of accessory pigments to chlorophyll-a, as the accessory pigments are known to absorb significantly higher amount of light in the blue region than in the red region of the spectrum [26]. Similar trends are seen for $a^*_{PHY}(\lambda)$ with chlorophyll-a concentration over the whole visible spectrum. These results have a large effect when parameterization of $a_{PHY}(\lambda)$ is done based solely on the concentration of the main pigment. For remote sensing applications involving empirical algorithms, the change in pigment composition and/or packaging effect influenced $R_{rs}(\lambda)$ ratios, however this effect would be subtle as compared to the effect of the bulk absorption properties. Empirical algorithms that utilize blue (412 nm or 443 nm or 490 nm) to green (555 nm or 560 nm) $R_{rs}(\lambda)$ ratios to estimate chlorophyll-a concentration, are overestimated when $a^*_{PHY}(\lambda)$ is lower which results in chlorophyll-a concentrations to be underestimated in the study region [27]. Further, even the semi-analytical algorithms like Carder, GSM01 and QAA algorithm are affected by $a^*_{PHY}(\lambda)$ variability as they use $R_{rs}(\lambda)$ ratios for estimation of absorption.

Table 1. Coefficients, R^2 and number of samples (n) for the power fit expressed as $a_x(443) = A_x(443)*[\text{chlorophyll-a}]^B x^{(443)}$. Where x = P - particulate absorption or PHY – phytoplankton absorption.

	This study (ANOVA; p<0.0001)				**Bricaud et al., 1998 [19]**			**Matsuoka et al., 2007 [20]**		
	A	**B**	**R^2**	**n**	**A**	**B**	**R^2**	**A**	**B**	**R^2**
$a_{PHY}(443)$ vs chlorophyll-a	0.0275	0.741	0.75	45	0.0378	0.627	0.90	0.0288	0.820	0.80
$a_P(443)$ vs chlorophyll-a	0.060	0.772	0.70	45	0.0520	0.635	0.91	0.0403	0.659	0.75

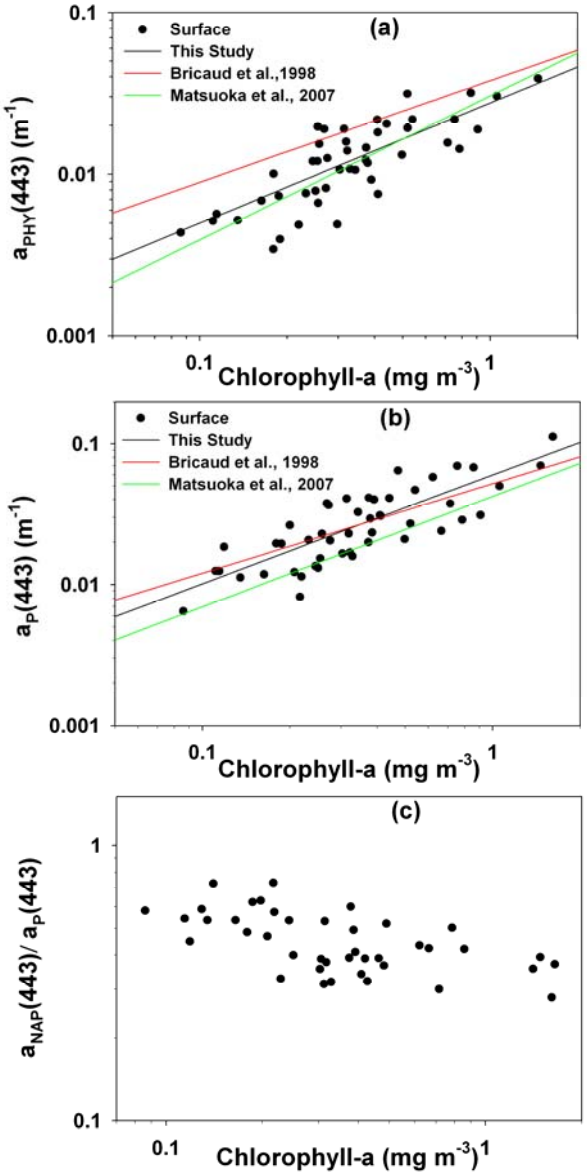

Fig. 3. Power fit applied to (a) phytoplankton absorption, $a_{PHY}(443)$, and (b) particulate absorption, $a_P(443)$, and chlorophyll-a relation, (c) ratio of $a_{NAP}(443)$ to $a_P(443)$ versus chlorophyll-a. The red and blue solid lines are power fits derived from Refs. 19 and 20 are shown for comparison. The statistics are shown in Table 1.

3.4 Comparison of satellite retrieved and in-situ absorption

Use of satellite data in the study region, like other high latitude regions, are often hampered by frequent ice and cloud cover. The Bering Sea is essentially ice free during summers (our study period) but thick cloud cover limited the number of clear sky images. The MODIS and MERIS overpass and in-situ sampling time window was fixed at ± 8 hours for this analysis. Very few collocated stations were obtained for MODIS and are included in this analysis for qualitative and comparison purpose.

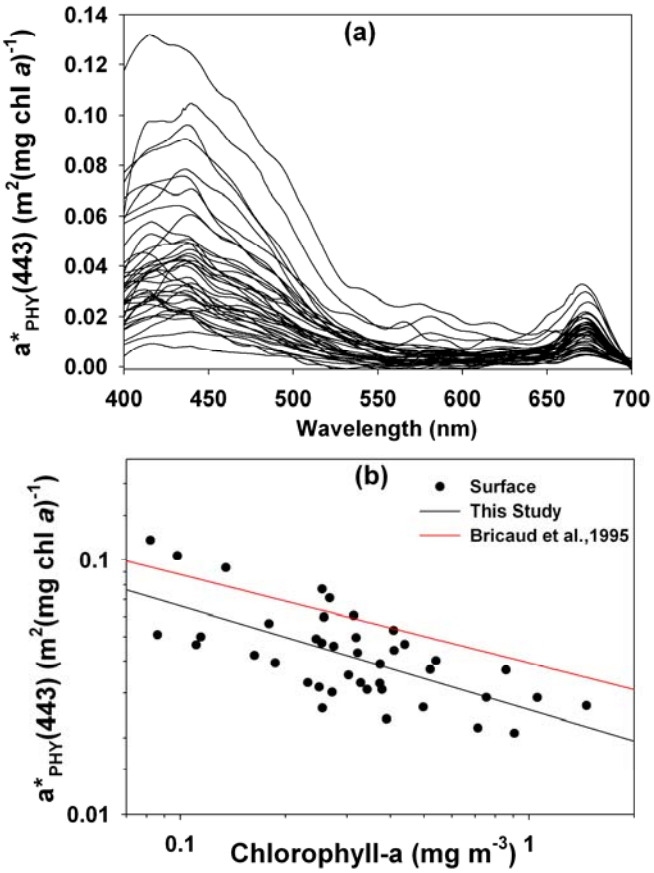

Fig. 4. Variability in (a) in-situ $a^*_{PHY}(\lambda)$ spectra for all stations, and (b) $a^*_{PHY}(443)$ with chlorophyll-a ($R^2 = 0.52$; N = 45, ANOVA; $p < 0.0001$). The red solid line is the fit obtained from Ref. 19 is shown for comparison.

The total absorption ($a_T(\lambda)$) and backscattering coefficients ($b_b(\lambda)$) control the spectral variability of $R_{rs}(\lambda)$ and can be expressed as

$$R_{rs}(\lambda) \approx \frac{b_b(\lambda)}{a_T(\lambda) + b_b(\lambda)}$$

The satellite retrieved $R_{rs}(\lambda)$ from MODIS and MERIS are shown in Fig. 5a and Fig. 5b, respectively. About half of the match-up stations showed blue and green reflectance's high and low, respectively, similar to other high latitude regions [2].

The Rrs(λ) spectra and total absorption minus absorption by pure water ($a_{T\text{-}W}(\lambda)$) spectra were separated into groups based on geographical locations (Fig. 1) along the transects CN, MN, SL and 70M (Fig. 5(c-j)). One way ANOVA and *post hoc* Tukey tests were conducted in MATLAB statistics toolbox 7.3 to find significance between groups. There were significant differences in magnitudes and spectral shapes of $R_{rs}(\lambda)$ in the blue region of the spectra along the transects (ANOVA; CN transect – $p = 0.002$, CN6 significantly different from CN8 and

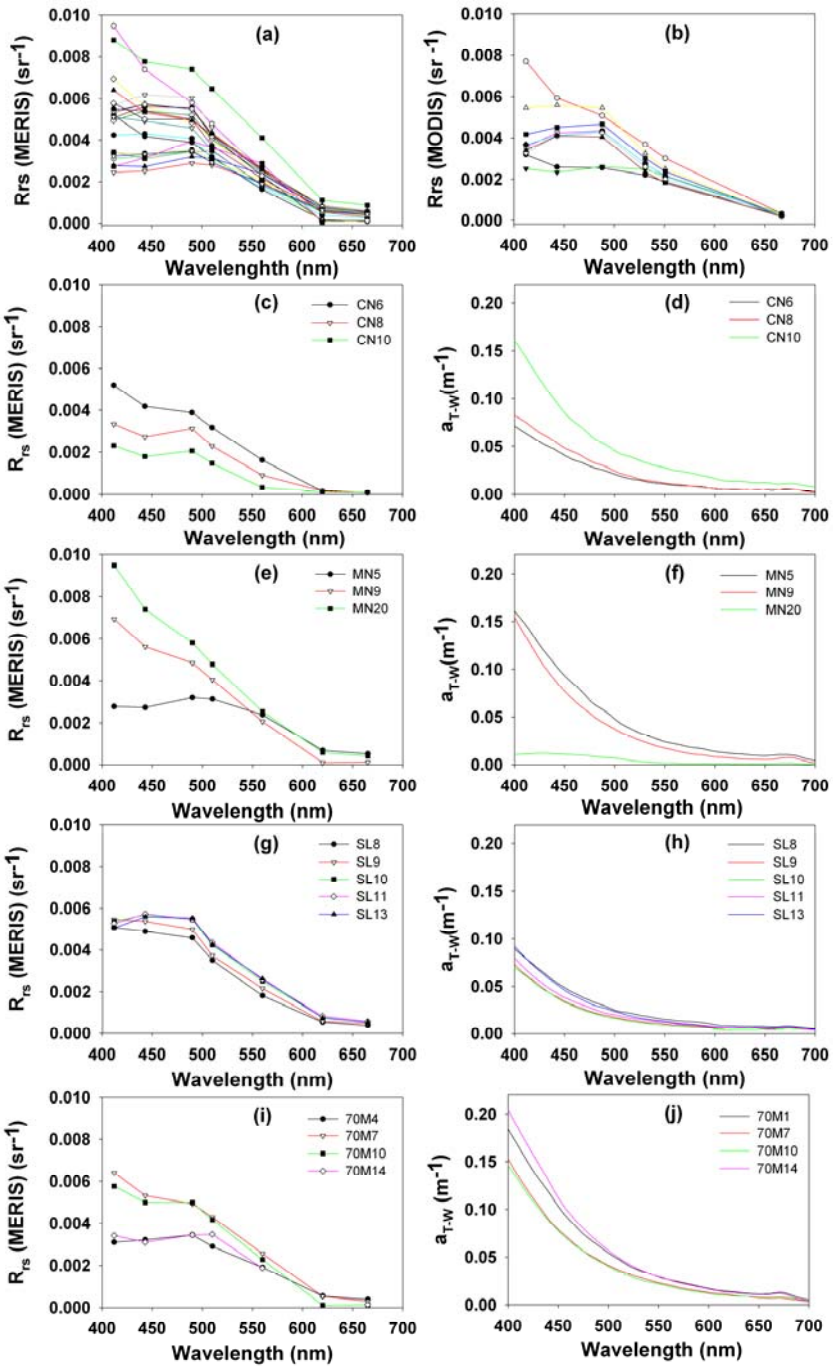

Fig. 5. Remote Sensing reflectance spectra ($R_{rs}(\lambda)$) from (a) MERIS, and (b) MODIS ocean color sensors. Comparison of MERIS $R_{rs}(\lambda)$ and in-situ $a_{T\text{-}W}(\lambda)$ for (c-d) CN transect, (e-f) MN transect, (g-h) SL transect, and (i-j) 70M transect. Transect and station locations are shown in Fig. 1.

CN10, MN transect - p = 0.01, MN5 significantly different from MN20, SL transect - p = 0.004, SL8 significantly different from SL13, and 70M transect - p = 0.003, 70M4 significantly different from 70M7 and 70M10, 70M7 significantly different from 70M4 and 70M14) as well as across transects (ANOVA, p = 0.002, CN transect is significantly different from MN and SL transect), which show that different types of water masses exist in the study region. This is supported by the corresponding varied $a_{T\text{-}W}(\lambda)$ obtained in the study area. The lowest values of $a_{T\text{-}W}(\lambda)$ and corresponding highest values of $R_{rs}(\lambda)$ were obtained for the most offshore stations where the clearest waters were found containing lowest biomass levels and in-situ particulate absorption. At these stations the $R_{rs}(\lambda)$ are known to be most influenced by $a_{NAP}(\lambda)$ and $a_{CDOM}(\lambda)$ rather than $a_{PHY}(443)$. So, the total absorption coefficient of surface waters often dominates the variability of $R_{rs}(\lambda)$ in our study. Hence absorption properties can be retrieved using simple reflectance ratios or semi-analytical algorithms. We will focus on comparing in-situ and satellite derived $a_{PHY}(\lambda)$ and $a_{DG}(\lambda)$.

3.4.1 Variation of $a_{PHY}(\lambda)$ and $a_{DG}(\lambda)$ with MERIS retrieved $R_{rs}(\lambda)$ band ratios

Empirical methods in which band ratios of ocean $R_{rs}(\lambda)$ are related to surface water properties such as chlorophyll-a concentration, absorption, suspended matter are common in ocean color remote sensing [28, 29]. The basic thought behind selecting and examining these band combinations and ratios is that variations in $R_{rs}(\lambda)$ at the blue wavelengths are strongly

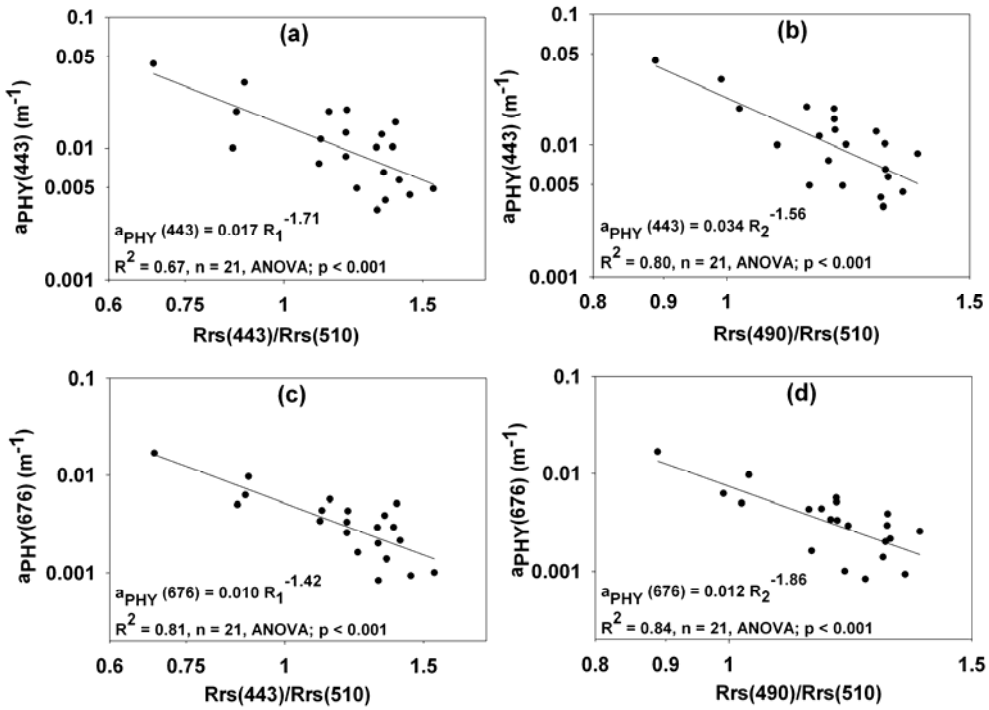

Fig. 6. Relationships between $a_{PHY}(\lambda)$ at 443 nm and the blue-to-green ratio of $R_{rs}(\lambda)$. (a) $a_{PHY}(443)$ versus $R_{rs}(443)/R_{rs}(510)$ (R_1), (b) $a_{PHY}(443)$ versus $R_{rs}(490)/R_{rs}(510)$ (R_2), (c) $a_{PHY}(676)$ versus $R_{rs}(443)/R_{rs}(510)$ (R_1), and (d) $a_{PHY}(676)$ versus $R_{rs}(490)/R_{rs}(510)$ (R_2). The least squares fit (solid lines and equations), the R^2 for log-transformed data, and the number of observations (n) are shown.

affected by absorption and variations in $R_{rs}(\lambda)$ at the green wavelengths are the most affected by light scattering by particles. The ratio of two bands reduces the effect of factors such as measurement geometry and atmosphere on the retrieval [28]. From a different perspective, the $R_{rs}(\lambda)$ band ratio is approximately equal to the product of backscattering ratio and absorption ratio [30] and can be expressed as

$$\frac{R_{rs}(\lambda_1)}{R_{rs}(\lambda_2)} \approx \left[\frac{b_b(\lambda_1)}{b_b(\lambda_2)}\right]\left[\frac{a_T(\lambda_2)}{a_T(\lambda_1)}\right]$$

So variations in $R_{rs}(\lambda)$ band ratios are driven primarily by the variability in backscattering and absorption. We didn't look at the backscattering properties and its influence on $R_{rs}(\lambda)$ in this study, however from Fig. 5(c-j) it appears that the $R_{rs}(\lambda)$ spectra are mostly influenced by absorption. Hence, we can examine this variability by relating $R_{rs}(\lambda)$ ratios and absorption. We used simple $R_{rs}(\lambda)$ band ratios on MERIS satellite data for deriving $a_{PHY}(\lambda)$ at 443 nm and 676 nm; which are the main absorption peaks in $a_{PHY}(\lambda)$ spectra (Fig. 6).

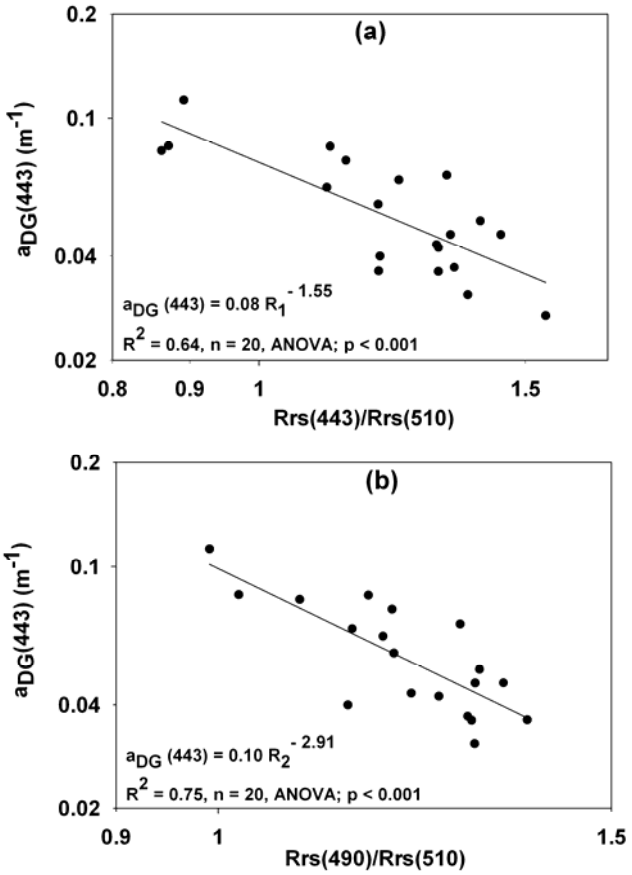

Fig. 7. Relationships between $a_{DG}(\lambda)$ at 443 nm and the blue-to-green ratio of $R_{rs}(\lambda)$. (a) $a_{DG}(443)$ versus $R_{rs}(443)/R_{rs}(510)$ (R_1), and (b) $a_{DG}(443)$ versus $R_{rs}(490)/R_{rs}(510)$ (R_2). The least squares fit (solid lines and equations), the R^2 for log-transformed data, and the number of observations (n) are shown.

Further, the in-situ $a_{PHY}(443)$ can be correlated to in-situ $a_{PHY}(\lambda)$ at other wavelengths using empirical relationships in the study region. For example the following relationship was obtained between in-situ $a_{PHY}(443)$ and in-situ $a_{PHY}(490)$

$$a_{PHY}(490) = 0.38[a_{PHY}(443)] + 0.55[a_{PHY}(443)]^2$$
$$(R^2 = 0.98;\ n = 65)$$

Different combinations of band ratios were tested; the band ratios that gave highest R^2 were selected i.e. $R_{rs}(443)/R_{rs}(510)$ (R_1) and $R_{rs}(490)/R_{rs}(510)$ (R_2). A simple 1st order inverse power fit was applied to $a_{PHY}(\lambda)$ at 443 nm and 676 nm and the reflectance ratios. The R_2 reflectance band ratio yielded the best results showing good correlations with $a_{PHY}(\lambda)$ at 443 nm and 676 nm (Fig. 6b and Fig. 6d). Irrespective of the band ratio used the relationship between $a_{PHY}(443)$ and the band ratio was similar; with the band ratios in general increasing as $a_{PHY}(443)$ decreased. In most analytical or semi-analytical models, the NAP/detrital and CDOM components are considered together as they have similar spectral shape [10,31]. Various band ratios were related to $a_{DG}(443)$ through a 1st order inverse power fit (Fig. 7). The $a_{DG}(443)$ was selected as it correlated well with $a_{DG}(\lambda)$ at other wavelengths using the spectral slope parameter (S_{DG}). For example in-situ $a_{DG}(412)$ can be calculated from in-situ $a_{DG}(443)$ using the mean value of in-situ $S_{DG} = 0.015 \pm 0.003$ as shown below

$$a_{DG}(412) = a_{DG}(443)e^{(-0.015(\lambda - 443))}$$
$$(R^2 = 0.95;\ n = 65)$$

The highest R^2 were obtained for $R_{rs}(443)/R_{rs}(510)$ (R_1) and $R_{rs}(490)/R_{rs}(510)$ (R_2). The R_2 ratio performed the best as compared to the other band ratios (Fig. 7b). Comparing the contribution of $a_{PHY}(443)$ and $a_{DG}(443)$ to R_2, the contribution of the non-pigmented (exponent = -2.91, Fig. 7) component was on an average higher than phytoplankton absorption (exponent = -1.55, Fig. 6).

These results suggested that the variations between two band reflectance ratios could be used to retrieve $a_{PHY}(443)$, $a_{PHY}(676)$ and $a_{DG}(443)$ in the study region. The number of data points (21) is statistically insufficient to establish robust algorithms, however it points out the future potential of this approach.

3.4.2 $a_{PHY}(\lambda)$ and $a_{DG}(\lambda)$ derived using QAA from MERIS and MODIS retrieved $R_{rs}(\lambda)$

Stations for which the QAA algorithm did not retrieve positive values of absorption at all wavelengths less than 580 nm were excluded from the comparison analysis. Absorption at wavelengths greater than 580 nm will not be analyzed as the QAA algorithm returns negative values at these wavelengths. The reason for the negative values is described in Lee et al. (2004) [32]. In brief, at wavelengths greater than 580 nm the total absorption coefficient is mostly dominated by pure water absorption with very little contribution of $a_{PHY}(\lambda)$, hence $a_{PHY}(\lambda)$ cannot be determined accurately from $R_{rs}(\lambda)$ at these wavelengths. The match-ups of in-situ and MERIS retrieved $a_{PHY}(\lambda)$ using QAA after log-transformation showed reasonable agreement with R^2 ranging from 0.50 – 0.71 and slope ranging from 0.77 to 0.87 at all wavelengths (Fig. 8, Table 2). More importantly $a_{PHY}(443)$ which corresponds to the maximum of $a_{PHY}(\lambda)$ spectra and is correlated to chlorophyll-a (Fig. 3a) was retrieved relatively more accurately (RMSE = 0.316) as compared to other wavelengths.

Table 2. Slope, R^2 and RMSE for the linear fit (ANOVA; $p < 0.001$) expressed as $a_{PHY}(\lambda)$ (in-situ) = $A_{PHY}(\lambda)$*[$a_{PHY}(\lambda)$ (satellite retrieved – MERIS/MODIS)].

Wavelength	A_{PHY}(slope)	R^2	RMSE	n
MERIS				
413 nm	0.83	0.70	0.242	18
443 nm	0.78	0.71	0.316	18
490 nm	0.77	0.50	0.431	18
510 nm	0.87	0.50	0.542	18
560 nm	0.82	0.50	0.674	18
All	0.82	0.74	0.503	90
MODIS				
410 nm	0.84	0.89	0.255	5
443 nm	0.77	0.75	0.382	5
490 nm	0.73	0.62	0.489	5
530 nm	0.79	0.86	0.378	4
550 nm	0.86	0.90	0.476	4
All	0.83	0.80	0.525	23

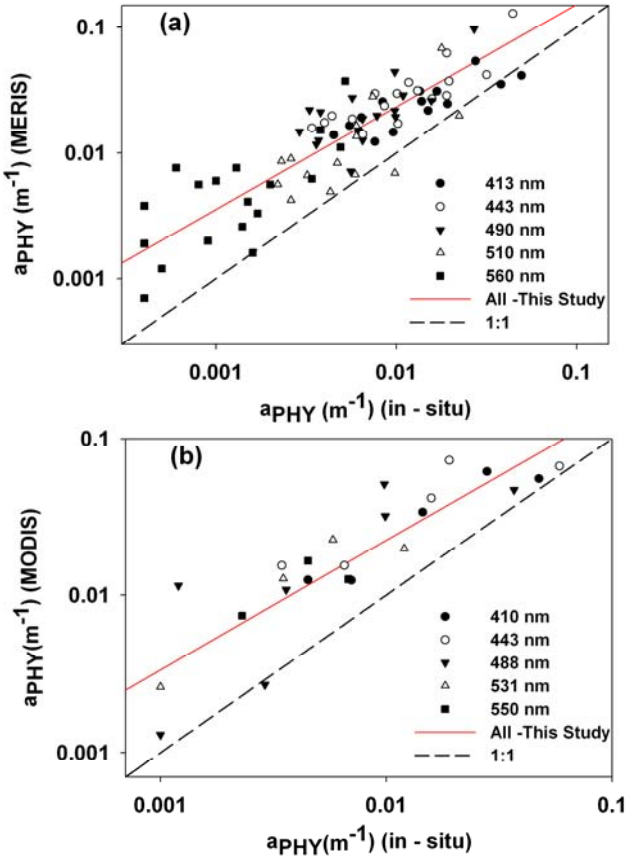

Fig. 8. Relationship between log-transformed in-situ $a_{PHY}(\lambda)$ versus QAA retrieved (a) MERIS $a_{PHY}(\lambda)$, and (b) MODIS $a_{PHY}(\lambda)$. Statistics of the linear fit for each wavelength are shown in Table 2.

The retrievals in the blue wavelengths were better than the green wavelength as $a_{PHY}(\lambda)$ usually shows a maximum in the blue region and a minimum in the green region of the spectra. In general, the QAA derived $a_{PHY}(\lambda)$ from MERIS overestimated $a_{PHY}(\lambda)$ at all wavelengths analyzed; a likely reason for this could be pigment packaging or change in pigment composition which leads to lower phytoplankton absorption and thus to higher Rrs(λ) [33] (discussed later). The match-ups of in-situ and MODIS retrieved $a_{PHY}(\lambda)$ using QAA after log-transformation showed much better agreement, but was not statistically reliable due to small sample size (n = 5). However, at all wavelengths except 490 nm, R^2 ranged from 0.75 – 0.90 and slope ranged from 0.77 – 0.86. The relationship between in-situ $a_{PHY}(\lambda)$ and QAA derived $a_{PHY}(\lambda)$ from MERIS as well as MODIS at all wavelengths showed reasonable agreement (Table 2).

The QAA does not retrieve NAP/detrital absorption but retrieves NAP/detrital plus CDOM ($a_{DG}(\lambda)$) absorption. For the purpose of match-up analysis the CDOM absorption was added to the NAP/detrital absorption. Fig. 9 shows the match-up of in-situ and QAA derived satellite $a_{DG}(\lambda)$ for MERIS and MODIS. Wavelengths greater than 580 nm were not included in the analysis as beyond 600 nm $a_{DG}(\lambda)$ values are very low due to the typical exponential decrease with increasing wavelength of $a_{DG}(\lambda)$ spectra.

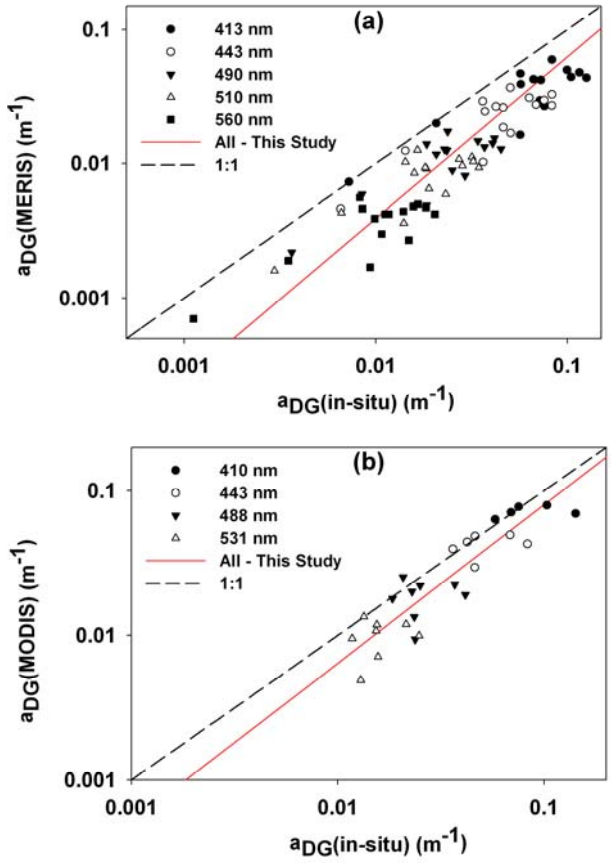

Fig. 9. Relationship between log-transformed in-situ $a_{DG}(\lambda)$ versus QAA retrieved (a) MERIS $a_{DG}(\lambda)$, and (b) MODIS $a_{DG}(\lambda)$. Statistics of the linear fit for each wavelength are shown in Table 3.

Table 3. Slope, R^2 and RMSE for the linear fit (ANOVA; $p < 0.001$) expressed as $a_{DG}(\lambda)$ (in-situ) = $A_{DG}(\lambda)$*[$a_{DG}(\lambda)$ (satellite retrieved – MERIS/MODIS)].

Wavelength	A_{DG}(slope)	R^2	RMSE	n
MERIS				
413 nm	1.11	0.60	0.401	18
443 nm	1.15	0.61	0.391	18
490 nm	1.16	0.61	0.381	18
510 nm	1.16	0.58	0.388	18
560 nm	1.18	0.44	0.433	18
All	1.16	0.84	0.416	90
MODIS				
All	1.01	0.80	0.362	27

The satellite retrieved $a_{DG}(\lambda)$ is consistent with in-situ data in terms of lower wavelengths showing higher absorption and higher wavelengths showing lower absorption after log-transformation. However $a_{DG}(\lambda)$ retrieved from MODIS did not statistically fit into a linear relationship with in-situ $a_{DG}(\lambda)$ at every wavelength, but over the entire waveband a good linear fit was obtained with $R^2 = 0.80$, slope = 1.01 and RMSE = 0.362 (Table 3). The $a_{DG}(\lambda)$ retrieved from MERIS shows better agreement with in-situ data at lower wavelengths than at higher wavelengths as seen from the decrease in R^2 and increase in RMSE values with increasing wavelength (Table 3). The QAA retrieved $a_{DG}(\lambda)$ from MERIS underestimated in-situ $a_{DG}(\lambda)$ at all wavelengths. The relationship of in-situ $a_{DG}(\lambda)$ and QAA derived $a_{DG}(\lambda)$ from MERIS at all wavelengths showed good agreement (Table 3). However at higher wavelengths few outliers along the 1:1 line could have influenced the relationship (Fig. 9).

The inconsistencies in match-up of both $a_{PHY}(\lambda)$ and $a_{DG}(\lambda)$ could be due to a few limitations in the QAA derivation of $a_{PHY}(\lambda)$ and $a_{DG}(\lambda)$. One of the limitations is the choice of spectral slope of CDOM and NAP/detrial absorption (S_{DG}). The QAA was run using the standard input for S_{DG} which was calculated from $R_{rs}(\lambda)$ for all collocated points. S_{DG} is known to be variable in natural systems ranging from 0.01 – 0.02 nm^{-1} [34]. Ideally S_{DG} values corresponding to the stations should be used which cannot be accurately determined using just $R_{rs}(\lambda)$ values [32]. To evaluate the effect of S_{DG} we calculated in-situ S_{DG} values from in-situ $a_{DG}(\lambda)$ by applying an exponential fit. The QAA was run with the in-situ S_{DG} to obtain $a_{PHY}(\lambda)$ and $a_{DG}(\lambda)$, however there was not much change in the retrieval of $a_{PHY}(\lambda)$ and $a_{DG}(\lambda)$. The average percent difference between QAA retrieved $a_{PHY}(\lambda)$ or $a_{DG}(\lambda)$ with fixed S_{DG} and QAA retrieved $a_{PHY}(\lambda)$ or $a_{DG}(\lambda)$ in-situ S_{DG} was ~7% at all wavelengths.

The other major factor that likely influenced the QAA outputs is the pigment packaging or change in pigment composition seen in our study. The low $a^*_{PHY}(\lambda)$ especially at stations where $a_{PHY}(\lambda)$ dominates the total absorption could result in increased $R_{rs}(\lambda)$ in the blue region leading to higher blue to green reflectance ratios. The blue to green reflectance ratios ($R_{rs}(443)/R_{rs}(560)$ for our study) are used in QAA to get $a_{PHY}(411)/a_{PHY}(443)$ and $a_{DG}(411)/a_{DG}(443)$, that are finally used to decompose $a_{PHY}(\lambda)$ and $a_{DG}(\lambda)$ from total water absorption [10, http://www.ioccg.org/groups/ Software_OCA/QAA_v5.pdf]. Higher blue to green ratios would result in lower $a_{PHY}(411)/a_{PHY}(443)$ and $a_{DG}(411)/a_{DG}(443)$ [10]. The mean value of $a_{PHY}(411)/a_{PHY}(443)$ and $a_{DG}(411)/a_{DG}(443)$ from in-situ data was 0.90±0.21 and 1.60±0.18 while the QAA gave a mean value of 0.81±0.02 and 1.55±0.17. In the QAA the difference between $a_{PHY}(411)/a_{PHY}(443)$ and $a_{DG}(411)/a_{DG}(443)$ is inversely related to $a_{DG}(\lambda)$

[10]. This difference as estimated by QAA is larger than in-situ resulting in underestimation of $a_{DG}(\lambda)$, and hence overestimation of $a_{PHY}(\lambda)$ by QAA relative to in-situ values.

In determination of $a_{PHY}(\lambda)$ values using the QFT method there is uncertainty in the 'Beta factor (β)' which can cause errors of about 10 – 20% [31]. Lee et al., (2004) [32] found that even when in-situ $R_{rs}(\lambda)$ was used as input to QAA an average percent difference of 21.4% existed between derived $a_{PHY}(\lambda)$ and in-situ $a_{PHY}(\lambda)$. Also in-situ $a_{PHY}(\lambda)$ and $a_{DG}(\lambda)$ are from discrete water samples whereas the QAA derived $a_{PHY}(\lambda)$ and $a_{DG}(\lambda)$ are integrated over the near surface upper water column [35]. Considering these uncertainties the match-up results obtained in this study are encouraging and can be used to determine $a_{PHY}(\lambda)$ and $a_{DG}(\lambda)$ from $R_{rs}(\lambda)$ at wavelengths ranging from 400 – 500 nm.

4 CONCLUSION

The total particulate and phytoplankton absorption coefficient in southeastern Bering Sea are well correlated with chlorophyll-a and are lower as a function of chlorophyll-a compared to low latitude regions. Variable specific phytoplankton absorption spectra with more variability in the blue than in the red part of the spectrum indicated change in pigment composition or package effect. There were significant differences in the magnitudes and spectral shapes of $R_{rs}(\lambda)$ spectra, which indicate that different types of waters exist in the study region. This was supported by the varied $a_{T\text{-}W}(\lambda)$ spectra obtained in study area. About half of our $R_{rs}(\lambda)$ spectra showed blue and green reflectances that were high and low, respectively. Simple two band ratios involving $R_{rs}(\lambda)$ ratios can be used to examine variability and retrieve $a_{PHY}(\lambda)$ from MERIS at 443 nm and 676 nm in the study region with $R_{rs}(490)/R_{rs}(510)$ giving best results. Similarly for $a_{DG}(\lambda)$ reflectance band ratio of $R_{rs}(490)/R_{rs}(510)$ could be used in the study region. The match-ups of in-situ and MERIS retrieved $a_{PHY}(\lambda)$ using QAA after log-transformation showed reasonable agreement. In general the QAA derived $a_{PHY}(\lambda)$ from MERIS overestimated in-situ $a_{PHY}(\lambda)$ at all wavelengths analyzed. The satellite retrieved $a_{DG}(\lambda)$ is consistent with in-situ data in terms of lower wavelengths showing higher absorption and higher wavelengths showing lower absorption. The QAA retrieved $a_{DG}(\lambda)$ from MERIS underestimated in-situ $a_{DG}(\lambda)$ at all wavelengths. The inconsistencies seen in the match-up analysis could be ascribed to uncertainties in the QFT method, discrete (in-situ) versus integrated (satellite) absorption coefficients comparison and change in pigment composition or package effect. Taking into account these errors the results obtained from the match-up analysis are encouraging and can be used for identification of major pigments and modeling purposes.

The results in this paper are obtained using a seasonally-limited in situ data set collected in July, 2008. The effects on the results during other seasons where relative contributions to absorption by phytoplankton and NAP/detrital matter varies from the conditions captured during the July 2008 sampling needs to be determined. Future applications would require optimization of the input parameters to the QAA. Also the satellite overpass and in-situ sampling time window could be increased so as to get more collocated data points.

Acknowledgments

This study was funded by NASA grant No: NNX07AR15G. The authors would like to thank Dr. Ray Sambrotto for the opportunity to participate in the BEST funded research cruise on the USCGC Healy.

References

[1] G. F. Cota, J. Wang, and J. C. Comiso, "Transformation of global satellite chlorophyll retrievals with a regionally tuned algorithm," *Remote Sens. Environ*. **90**, 373– 377(2004) [doi:10.1016/j.rse.2004.01.005].

[2] H. M. Dierssen and R.C. Smith, "Bio-optical properties and remote sensing ocean color algorithms for Antarctic Peninsula waters," *J. Geophys. Res.* **105**, 26301–26312 (2000) [doi:10.1029/1999JC000296].

[3] M. J. Behrenfeld, E. Boss, D. A. Siegel, and D. M. Shea, "Carbon based ocean productivity and phytoplankton physiology from space," *Global Biogeochem. Cycles* **19**, GB1006 (2005) [doi:10.1029/2004GB002299].

[4] J .L. Mueller, "SeaWiFS algorithm for the diffuse attenuation coefficient, K (490), using water-leaving radiances at 490 and 555 nm," *SeaWiFS Postlaunch Calibration and Validation Analyses,* Part 3, vol. 11, S. B. Hooker and E. R. Firestone, Eds., Rep. NASA/TM-2000– 206892, pp. 24–27, NASA Goddard Space Flight Cent, Greenbelt, MD (2000).

[5] E .J. Rochelle-Newall and T. R. Fisher, "Production of chromophoric dissolved organic matter fluorescence in marine and estuarine environments: An investigation into the role of phytoplankton," *Mar. Chem.* **77**, 7– 21 (2002) [doi:10.1016/S0304-4203(01)00072-X].

[6] M. A. Springer, C. P. McRoy, and V. M. Flint, "The Bering Sea Green Belt: shelf-edge processes and ecosystem production," *Fish. Oceanogr.* **5**, 205–223 (1996) [doi:10.1111/j.1365-2419.1996.tb00118.x].

[7] S. R. Hare and N. J. Mantua, "Empirical evidence for North Pacific regime shifts in 1977 and 1989," *Prog. Oceanog.* **47**, 103-145 (2000) [doi:10.1016/S0079-6611(00)00033-1].

[8] T. Iida and S. Saitoh, "Temporal and spatial variability of chlorophyll concentrations in the Bering Sea using empirical orthogonal function (EOF) analysis of remote sensing data," *Deep Sea Res. II* **54**, 2657-2671 (2007) [doi:10.1016/j.dsr2.2007.07.031].

[9] N. B. Kachel, G. L. Hunt Jr., S. A. Salo, J. D. Schumacher, P. J. Stabeno, and T. E. Whitledge, "Characteristics and variability of the inner front of the southeastern Bering Sea," *Deep Sea Res. II* **49** (26), 5889–5909 (2002) [doi:10.1016/S0967-0645(02)00324-7].

[10] Z. P. Lee, K. L. Carder, and R. Arnone, "Deriving inherent optical properties from water color: A multi-band quasi-analytical algorithm for optically deep waters," *Appl. Opt.* **41**, 5755– 5772 (2002) [doi:10.1364/AO.41.005755].

[11] B. G. Mitchell, "Algorithms for determining the absorption coefficients for aquatic particulates using the quantitative filter technique," *Proc. SPIE* **1302**, 137–148, (1990) [doi:10.1117/12.21440].

[12] M. Kishino, M. Takahashi, N. Okami, and S. Ichimura, "Estimation of the spectral absorption coefficients of phytoplankton in a thermally stratified sea," *Bull. Mar. Sci.* **37**, 634–642 (1985).

[13] G. Mitchell, A. Bricaud, K. Carder, J. Cleveland, G. Ferrari, R. Gould, M. Kahru, M. Kishino, H. Maske, T. Moisan, L. Moore, N. Nelson, D. Phinney, R. Reynolds, H. Sosik, D. Stramski, S. Tassan, C. Trees, A. Weidemann, J. Weiland, and A. Vodacek, "Determination of spectral absorption coefficients of particles, dissolved material, and phytoplankton for discrete water samples," in *Ocean optics protocols for satellite ocean color sensor validation, Revision 2, NASA/TM 2000-209966*, G. S. Fargion and J. L. Mueller, Eds, pp. 125-153, NASA, Goddard Space Flight Center, Greenbelt, MD (2002).

[14] J. S. Cleveland and A. D. Weidemann, "Quantifying absorption by aquatic particles: a multiple scattering correction for glass fiber filters," *Limnol. Oceanogr.* **38**, 1321-1327(1993) [doi:10.4319/lo.1993.38.6.1321].

[15] O. Holm-Hansen, C. J. Lorenzen, R. W. Holmes, and J. D. H. Strickland, "Fluorometric determination of chlorophyll," *ICES J. Marine Sci.* **30**, 3-l5 (1965) [doi:10.1093/icesjms/30.1.3] .

[16] H. R. Gordon and K. J. Voss, "MODIS normalized water-leaving radiance algorithm. MODIS Algorithm Theoretical Basis Document 18," (1999) http://modis.gsfc.nasa.gov/data/atbd/atbd_mod18.pdf
[17] P. J. Stabeno, N. B. Kachel, C. W. Mordy, D. Righi, and S. A. Salo, "An examination of the physical variability around the Pribilof Islands, 2004," *Deep Sea Res.* **55**, 1701-1716 (2008) [doi:10.1016/jdsr2.2008.03.006].
[18] P. Naik, E. J. D'Sa, J. Goes, and H. R. Gomes, "Particulate absorption properties from MODIS Ocean color and four in-situ transects in the southeastern Bering Sea shelf during July, 2008," *Proc. SPIE* **7473**, 747302 (2009a) [doi:10.1117/12.831351].
[19] P. Naik, E. J. D'Sa, J. Goes, and H. R. Gomes, "Absorption properties along the 70-m isobath in the southeastern Bering Sea during July 2008," *Proc. IEEE/MTS Oceans 2009*, 1-7 (2009b).
[20] A. Bricaud, A. Morel, M. Babin, K. Allali, and H. Claustre, "Variations of light absorption by suspended particles with chlorophyll a concentration in oceanic (case 1) waters: analysis and implications for biooptical models," *J. Geophys. Res.* **103**, 31033–31044 (1998) [doi:10.1029/98JC02712].
[21] A. Matsuoka, Y. Huot, K. Shimida, S.-I Saitoh, and M. Babin, "Bio-optical characteristics in the Western Arctic Ocean: Implications for ocean color algorithms," *Canadian J. Remote Sens.* **33**, 503-518 (2007).
[22] J. Wang, G. F. Cota, and D. A. Ruble, "Absorption and backscattering in the Beaufort and Chukchi Seas," *J. Geophys. Res.* **110**, C04014 (2005) [doi:10.1029/2002JC001653].
[23] S. Sathyendranath, V. Stuart, B. D. Irwin, H. Maass, G. Savidge, L. Gilpin, and T. Platt, "Seasonal variations in bio-optical properties of phytoplankton in the Arabian Sea," *Deep Sea Res.* **46**, 633–654 (1999) [doi:10.1016/S0967-0645(98)00121-0].
[24] T. Fujiki and S. Taguchi, "Variability in chlorophyll a specific absorption coefficient in marine phytoplankton as a function of cell size and irradiance," *J. Plankton Res.* **24**, 859–874 (2003) [doi:10.1093/plankt/24.9.859].
[25] A. Bricaud, M. Babin, A. Morel, and H. Claustre, "Variability in the chlorophyll-specific absorption coefficients of natural phytoplankton: analysis and parameterization," *J. Geophys. Res.* **100**, 13321-13332 (1995) [doi:10.1029/95JC00463].
[26] S. E. Lohrenz, A. D. Weidemann, and T. Merritt, "Phytoplankton spectral absorption as influenced by community size structure and pigment composition," *J. Plankton Res.* **25**, 35-61 (2003) [doi:10.1093/plankt/25.1.35].
[27] F. E. Müller-Karger, C. R. McClain, R. N. Sambrotto, and G. C. Ray, "A comparison of ship and Coastal Zone Color Scanner mapped distributions of phytoplankton in the southeastern Bering Sea," *J. Geophys. Res.* **95**, 11483-11499 (1990) [doi:10.1029/JC095iC07p11483].
[28] J. E. O'Reilly, S. Maritorena, B. G. Mitchell, D. A. Siegel, K. L. Carder, S. A. Garver, M. Kahru, and C. McClain, "Ocean color algorithms for SeaWiFS," *J. Geophys. Res.* **103**, 24937-24953 (1998) [doi:10.1029/98JC02160].
[29] E. J. D'Sa, R. L. Miller, and B. A. McKee, "Suspended particulate matter dynamics in coastal waters from ocean color: applications to the northern Gulf of Mexico," *Geophys. Res. Lett*. **34**, L23611 (2007) [doi:10.1029/2007GL031192].
[30] H. R. Gordon, O. B. Brown, R. H. Evans, J. W. Brown, R. C. Smith, K. S. Baker, and D. K. Clark, "A semianalytic model of ocean color," *J. Geophys. Res.* **93**, 10909–10924 (1988) [doi:10.1029/JD093iD09p10909].
[31] K. L. Carder, F. R. Chen, Z. P. Lee, S. K. Hawes, and D. Kamykowski, "Semianalytic moderate-resolution imaging spectrometer algorithms for chlorophyll-

a and absorption with bio-optical domains based on nitrate-depletion temperatures," *J. Geophys. Res.* **104**, 5403– 5421 (1999) [doi:10.1029/1998JC900082].

[32] Z. P. Lee and K. L. Carder, "Absorption spectrum of phytoplankton pigments derived from hyperspectral remote-sensing reflectance," *Remote Sens. Environ*. **89**, 361-368 (2004) [doi:10.1016/j.rse.2003.10.013].

[33] K. L. Carder, F. R. Chen, S. K. Hawes, Z. P. Lee, and J. P. Cannizzaro, "MODIS Ocean Science Team Algorithm Theoretical Basis Document, ATBD 19, Case 2 Chlorophyll a," ATBD 19, version 7 (2003).

[34] J. T. O. Kirk, *Light and Photosynthesis in Aquatic Ecosystems*, Cambridge University Press, Cambridge, UK (1994).

[35] H. R. Gordon and D. K. Clark, "Remote sensing optical properties of a stratified ocean: an improved interpretation," *Appl. Opt.* **19**, 3428–3430 (1980) [doi:10.1364/AO.19.003428].